Romanian Reports in Physics, Vol. 68, Supplement, P. S447–S481, 2016

GAMMA BEAM DELIVERY AND DIAGNOSTICS

H.R. WELLER[1], C.A. UR[2], C. MATEI[2,a], J.M. MUELLER[1], M.H. SIKORA[1], G. SULIMAN[2], V. IANCU[2], Z. YASIN[2]

[1]Triangle Universities Nuclear Laboratory / Duke University, Durham, NC 27708, USA
[2]ELI-NP, "Horia Hulubei" National Institute for Physics and Nuclear Engineering, 30 Reactorului Street, RO-077125, Bucharest-Magurele, Romania
[a] Corresponding author *E-mail*: catalin.matei@eli-np.ro

Abstract. The high brilliance Gamma Beam System at ELI-NP is based on the Inverse Compton Scattering of laser light on relativistic electron bunches provided by a warm radio-frequency linear accelerator. The system will deliver quasi-monochromatic gamma-ray beams (bandwidth 0.5%) with a high spectral density (10,000 photons/s/eV) and high degree of linear polarization (99%). The system will be delivered by the EuroGammaS Association, a European consortium of academic and research institutions and commercial companies with well-established expertise in the field. Optimization and monitoring of the Gamma Beam System requires the proper means for accurately measuring the spatial, spectral and temporal characteristics of the gamma-ray beams. The system will be delivered by the EuroGammaS Association with a set of devices for the optimization of the gamma-ray beam characteristics to be used during the initial phase of setting up the system. The present TDR is dealing with additional equipment and techniques, complementary to the ones provided by EuroGammaS, required to deliver the gamma-ray beams to the experimental setups and to monitor the characteristics of the beams during the performance of the experiments. Consequently, there are two main categories of equipment to be considered: a) equipment for the delivery of the gamma-ray beam to users including beam pipes, vacuum systems, collimators, alignment platforms, shielding, and beam dumps; b) diagnostics and monitor devices to be used during the operation of the gamma beam system. An extensive description of the equipment and devices needed for beam delivery, diagnostics and monitoring is given in Section 2 of this document. The development, construction and installation of the delivery, diagnostic and monitoring equipment is strongly related to the phases of installation of the Gamma Beam System and the corresponding properties of the gamma-ray beam at each phase. The development and building of the devices is scheduled according to these phases. The development of beam diagnostics and monitor devices is done within an international collaboration and it will take advantage of the know-how elaborated at other gamma-ray beam facilities presently in operation such as HIγS at TUNL/Duke University.

Key words: ELI-NP, gamma beam transport, gamma beam diagnostics, polarization asymmetry, nuclear resonance fluorescence, Compton scattering.

1. INTRODUCTION

The ELI-NP project aims to open new dimensions in basic and applied nuclear physics research and material sciences applications with brilliant gamma-ray beams [1]. In designing a state-of-the-art gamma-ray beam system several requirements have to be fulfilled, such as: as small as possible bandwidth, strong increase of the peak brilliance and of the gamma beam flux, reduction of the gamma beam size. A careful analysis of the presently running gamma beam systems worldwide have revealed that the fulfillment of these requirements, with the present technology, is possible only by using the laser Compton backscattering (LCB) technique on relativistic electrons provided by a linear accelerator (LINAC). An example of such a gamma-ray source is T–REX at Lawrence Livermore National Laboratory [2]. The main advantage of using LINAC accelerators is the excellent emittance of the provided electron beams. This approach is based on the interaction of short laser pulses with relativistic electrons, *i.e.* inverse Compton scattering (ICS), to create ultra-bright quasi-monoenergetic gamma-ray beams. The scattered radiation is Doppler upshifted by more than 1,000,000 times and is forwardly-directed in a narrow, polarized, tunable, laser-like beam.

Advanced gamma-ray systems, based on Compton backscattering are considered to be the new roadmap to open the field of nuclear photonics. Such Compton colliders aim at producing extreme gamma-ray beams for nuclear physics and nuclear photonics experiments.

The High Brilliance Gamma Beam System (GBS) of ELI-NP will produce intense gamma-ray beams with spectral densities of about 10^4 γ/s/eV, a narrow bandwidth (0.5%), high degree of polarization (99%) and tunable energy in the range from 200 keV to 19.5 MeV [3]. The small dimension of the beam is required also because it is envisioned that the gamma-ray system will be used in conjunction with the low repetition rate ELI-NP 10 PW laser beams.

For the implementation of the ELI-NP gamma beam system the following two principles were used: 1) a staged realization that permits a sequential buildup of the facility according to the available resources, and 2) a flexible design in such a way as to accommodate its future growth.

To optimize the operation of a Compton light source and its use for experiments it is of utmost importance to have the proper means to accurately predict the spatial, spectral and temporal characteristics of the gamma beam. The present TDR is dealing with the equipment and techniques meant to optimize the gamma-ray beam at ELI-NP. Two main categories of equipment are considered: i) the delivery of the gamma-ray beam to users including collimators, shielding, beam dumps and diagnostics and ii) monitor of the beam features during the operation of the gamma beam system. An extensive description of the tools needed for the beam delivery, diagnostics and

monitor is given in Section 2.

The development of the delivery, diagnostic and monitor equipment is strongly related to the phases of installation of the GBS and the corresponding properties of the gamma-ray beam delivered at each phase. One needs to prioritize the development and building of the proper characterization tools according to these phases. The phases of the GBS installation are presented in Section 2.3.

2. THE GAMMA BEAM SYSTEM AT ELI-NP

The main criteria to define the Gamma Beam System for ELI-NP were: the energy of the gamma-ray beam, the spectral density, the peak brilliance and the bandwidth. The total photon flux is measured in photons/s/eV. The driving force behind the development of light sources is the optimization of their brilliance (or spectral brightness), which is the figure of merit of many experiments. Brilliance is defined as a function of frequency given by the number of photons emitted by the source in unit time, in a unit solid angle, per unit surface of the source, and in a unit bandwidth of frequencies around the given one. The units in which it is usually expressed are photons/s/mm^2/mrad^2/0.1%BW. The brilliance puts a premium not only on the photon flux (photons per second in a given bandwidth) but also on the high phase space density of the photons, *i.e.* on being radiated out of a small area and with high directional collimation. The gamma-ray beam bandwidth is the width of the range (or band) of frequencies in which the beam energy spectrum is concentrated. The ELI-NP Gamma Beam System will produce a very intense and brilliant gamma-ray beam ($E_\gamma = 0.2$-19.5 MeV) obtained from the incoherent Compton backscattering of laser light with a very brilliant and intense relativistic electron beam ($E_e \leq 0.7$ GeV). The experiments envisaged with the gamma-ray system put some limits on the parameters of the gamma-ray beam: bandwidth equal or lower than 5×10^{-3}, energy up to 19.5 MeV to access the Giant Dipole Resonance in most nuclei, spectral density of the order of 10^4 photons/s/eV, peak brilliance higher than 10^{21}photons/mm^2/mrad^2/s/(0.1%BW).

2.1. THE PRINCIPLE

The gamma-ray beam is produced through Compton backscattering of laser light off an accelerated electron beam. Laser photons with energy E_L are exploited to generate photon beams with high energies E_γ via Compton backscattering at a small angle θ_γ from a counter-propagating fast electron beam (see Fig. 1), characterized by

its relativistic factor according to the formula:

$$E_\gamma = 2\gamma_e^2 \frac{1+\cos\theta_L}{1+(\gamma_e\theta_\gamma)^2+a_0^2+\frac{4\gamma_e E_L}{mc^2}} E_L \tag{1}$$

where: $\frac{4\gamma_e E_L}{mc^2}$ – recoil parameter;
$a_L = \frac{eE}{m\omega_L c}$ – normalized potential vector of the laser field;
E = laser electric field strength; $E_L = \hbar\omega_L$

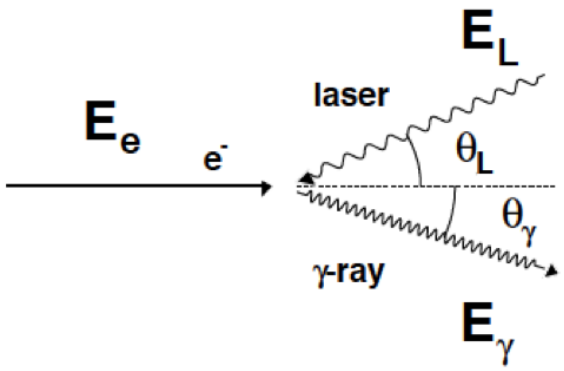

Fig. 1 – A schematic view of the Compton backscattering process of a laser beam with energy E_L off a relativistic electron beam with energy E_e. Here the general case of the Compton scattering is schematized where the laser beam direction collides with the electrons at an angle θ_L and the backscattered gamma beam is considered at the angle θ_γ.

The energy of the scattered gamma rays will be distributed between the minimum value (E_L) and the maximum Doppler upshift occuring at head-on collision (θ_L = 0°) and backscattering (θ_γ = 0°):

$$E_\gamma \approx 4\gamma_e^2 E_L. \tag{2}$$

2.2. DESCRIPTION OF GBS

The ELI-NP GBS is an advanced source of gamma-ray photons able to produce beams of monochromatic and high spectral density gamma-ray photons. The main specifications of the system are: photon energy tunable in the range 0.2–19.5 MeV, RMS bandwidth smaller than 0.5% and spectral density larger than 10^4 photons/s/eV, with source spot sizes of about 10–30 microns.

A schematic layout of the GBS is given in Fig. 2. The system will consist of two stages:

i) the low-energy stage in which electrons are accelerated to energies up to 300 MeV and gamma rays are produced with energies up to 3.5 MeV;

ii) the high-energy stage where electrons are accelerated up to 750 MeV and gamma rays are produced with energies up to 19.5 MeV.

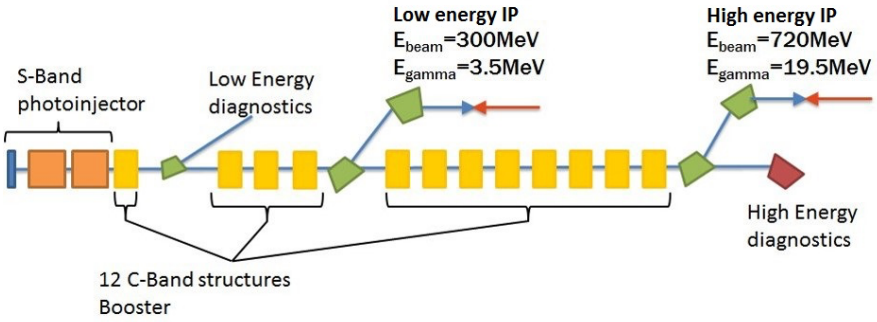

Fig. 2 – Layout of the ELI-NP Gamma Beam System. The source is based on a two stages warm LINAC electron accelerator providing gamma rays with energies up to 3.5 MeV and 19.5 MeV, respectively.

Every stage is equipped with a dedicated diagnostics system for tuning and beam optimization [3]. Fig. 3 illustrates the location of the GBS in the main experimental building. The whole system is located on an anti-vibrational platform aiming to decouple the system from any outside vibration. The limits of the anti-vibrational floor are marked with red in Fig. 3. The High Power Laser System (HPLS) and the experimental areas are located on the same platform. The platform and the anti-vibration mounts in the basement are also visible in the right-side of Fig. 3. The vibration platform is designed to keep the level of vibrations below 1 μm at 10 Hz. This level of vibrations is crucial for ensuring the proper interaction between the laser light and the electron beam.

The final parameters of the GBS are listed in Table 1. These parameters of the gamma beam have to be achieved for the full system, which will be operational in the second half of 2018. In an intermediate phase, planned to commence at the beginning of 2017, the system will consist of the low-energy stage and it will provide beams with energies below 3.5 MeV.

2.3. PHASES OF INSTALLATION

2.3.1. Low-energy gamma-rays phase

The intermediate stage of the project is planned to be operational in the first part of 2017. All necessary beam components should be installed in the low-energy

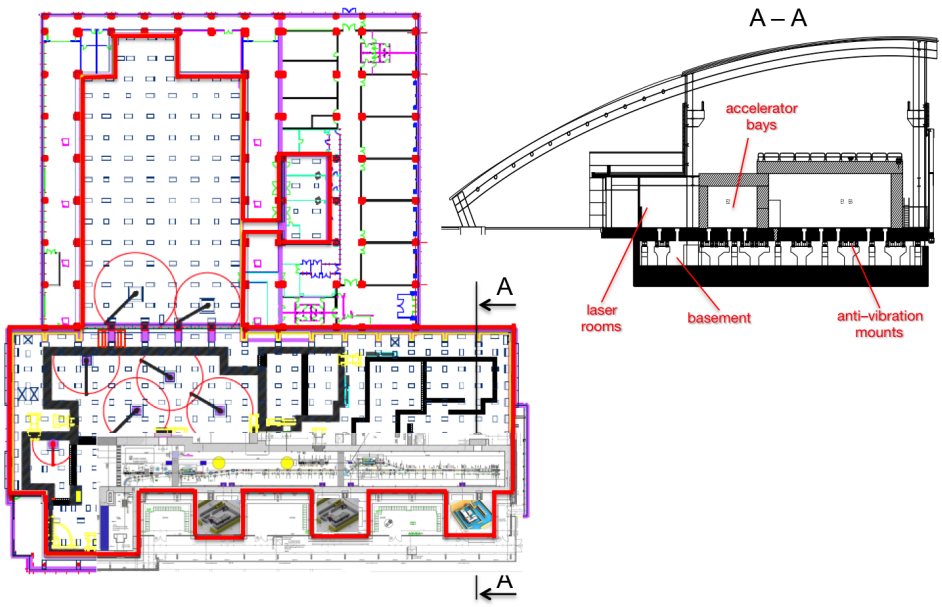

Fig. 3 – Location of the ELI-NP Gamma Beam System in the general layout of the ELI-NP experimental building. The limits of the anti-vibration platform are marked with the red line. A section through the building is shown on the right side.

Table 1

The parameters of the ELI-NP gamma-ray beam.

Parameter [units]	Value
Photon energy [MeV]	0.2–19.5
Spectral density [ph/s/eV]	$>10^4$
Bandwidth	<0.5 %
Nr photons per shot within FWHM bdw.	$1.0–4.0\cdot10^5$
Nr photons/sec within FWHM bdw.	$2.0–8.0\cdot10^8$
Source rms size [μm]	10–30
Source rms divergence [μrad]	25–250
Peak brilliance [Nph/sec.mm^{2}mrad^{2}0.1%]	$10^{22}–10^{24}$
Radiation pulse length [ps]	0.7–1.5
Linear polarization	>99 %
Macro repetition rate [Hz]	100
Nr of pulses per macropulse	>31
Pulse-to-pulse separation [ns]	16

experimental hall E2.

The gamma beam characteristics for this phase are:

- gamma rays of less than 3.5 MeV with BW of 0.5%
- beam spot diameter FWHM $\leq$ 1 cm

Several diagnostic tools should be ready at the end of this phase to monitor and characterize the gamma beam.

2.3.2. The full system

The full system providing the beam with the design parameters is expected to be ready in September 2018.

All diagnostics and monitor systems have to be already commissioned and ready to be used.

3. GAMMA BEAM DELIVERY AND DIAGNOSTICS

3.1. GAMMA BEAM DELIVERY

All the gamma beam transport will have to take place in vacuum because the high intensity of photons will lead to the creation of forward scattered clouds of electrons and photons which will otherwise impact the subsequent experimental targets and beam diagnostics. The total length of the beam transport line is approximately 100 m. The vacuum pipe will have a modular design, allowing the removal of individual segments for the placement of experimental apparatus. The pumping stations will be distributed according to their pumping power, making vacuum connections between sections of pipe where that is necessary.

In designing the gamma beam delivery system one has to keep in mind several requirements, as follows:

- beam transport should be made under vacuum to avoid background generation from the scattering on air
  - better than 10^{-3} mbar where there is no communication with the electron accelerator
  - better than 10^{-6} mbar where there is communication with the electron accelerator
- if possible beam diagnostic devices and collimators will be placed under vacuum

- all the in-air transport should be as short as possible and proper shielding should be installed for the devices downstream
- the passages vacuum-air-vacuum will be made through thin, low absorption, low scattering windows

3.1.1. Collimators

The small transversal dimension of the gamma-ray beam of about 5 mm FWHM (full width at half maximum) will pose a significant challenge in machining or casting collimators with lengths of 10–15 cm long. The alternative is to use same kind of collimators proposed by the EuroGammaS for the GBS; succession of several W dual-slit variable aperture systems [3]. This collimator is operated under vacuum and the aperture of the individual slits is controlled with stepper motors. Post collimation stage needs to be defined: sweeper magnet, concrete wall for neutrons produced in W or Pb.

3.1.2. Beam dumps

The beam dumps for the gamma-ray beam should ensure complete absorption of fast neutrons (when produced) and minimize the back scattering of radiation into the experimental vault. Two different types of beam dumps have to be built: one for low-energy gamma-ray beams up to 3.5 MeV and another one for high-energy gamma-ray beams up to 19.5 MeV.

Small beam dumps for the already collimated beam are going to be built at the exit from each of the experimental areas to ensure safety of work in the downstream rooms.

3.1.3. Shielding

Even when the beam line is under vacuum, the unprecedented gamma intensity creates a sizable flux of forward scattered electrons and lower energy photons. Most of these photons and electrons have larger divergence than the beam, so a thin lead shield will be used in front of each experimental area.

3.1.4. Secondary electrons removal

Secondary electrons originating at the collimators have the potential of creating unwanted background in the experimental systems and shall be removed from the direction of the gamma beam. This can be achieved by the use of a sweeper magnet after the collimator.

3.1.5. Alignment system

The total length of the low-energy beam transport line from the photon generation point to the low-energy dump in room E8 is 80 m. The high-energy beam

transport line measures 30 m from the photon generation point to the high-energy dump in E8. A laser system to ensure rapid and accurate alignment of the beam transport components and experimental target to the photon beam is needed at a position close to where the photon beam is generated. The laser beam will be directed along the beam transport line mimicking the photon beam path. Use of this tool will simplify alignment at the experimental stations, which could be completed before photon beam time begins.

3.2. GAMMA BEAM DIAGNOSTICS

As part of the tender procedure the EuroGammaS association is building a characterization system in order to assess the machine performance and monitor its parameters during the tuning procedures. Two similar beam characterization stations are foreseen, one for each gamma line. They are described in [3] and are summarized as consisting of five basic elements:

- beam flux monitor to measure and monitor the photon yield;
- beam position imager to spot the beam position for alignment and diagnostics purposes;
- Compton spectrometer, to measure the photon energy spectrum for monitoring purposes;
- sampling calorimeter for a fast combined measurement of the beam average energy and intensity, to be used during machine commissioning and development;
- resonant scattering spectrometer for absolute beam energy calibration and intercalibration of the other detector elements.

Each characterization station is situated after the main collimator, but before most of the experimental areas. Additionally, some of these diagnostics can only be operated during the tuning of the machine as they interfere with the beam. As a result, it is necessary to complement these measurements. We are proposing several real-time beam monitoring systems:

- energy and energy spread
- flux measurement
- beam polarization measurement
- spatial position monitor
- time structure monitor

3.2.1. Gamma beam energy spread

We are proposing a direct measurement of the beam energy spread using a large volume HPGe detector or a $LaBr_3$ detector with anti-Compton shield placed in the attenuated beam. This system will complement the out of beam measurement proposed by EuroGammaS.

The time structure and intensity of the ELI-NP γ-ray beams offers a significant challenge to measurements of the beam characteristics. Typical detectors such as NaI or HPGe placed in the beam would suffer significant pile-up effects and measurements would not be possible. One solution for in-beam measurements is to reduce the beam intensity using an attenuator similar to the system developed at HIγS [4]. The primary function of an attenuator system is to attenuate the γ-ray beam by a known amount.

In tests performed at HIγS it has been determined that the Cu attenuators have no measurable effect on the energy spread of the primary gamma-ray beam. The measurements have been carried out using a HPGe detector at an energy $E_\gamma = 8$ MeV [4].

3.2.2. Gamma beam flux

A. The d(γ,n)p intensity monitor and polarimeter

We propose an intensity and polarization monitor based on the d(γ,n)p which can be placed in either the low-energy or the high-energy experimental areas. The photodisintegration of the deuteron is one of the most-studied photonuclear reactions. Significant experimental and theoretical work has been done to better understand the differential cross section and the polarization asymmetry of the outgoing neutrons when using a linearly-polarized gamma-ray beam. This reaction is typically used as a benchmark for studies of the beam polarization and intensity for gamma-ray beams below 20 MeV. The d(γ,n) reaction has a large polarization asymmetry in the outgoing neutrons for beam energies between 2.5 and 20 MeV, as indicated by theoretical calculations [5] and confirmed by experimental measurements [6].

The threshold for photodisintegration of the deuteron is 2.23 MeV. In order to have significant energies in the neutrons, this reaction can be used at energies of 2.5 MeV and above. In addition, the analyzing power goes to zero at threshold, but rises to about 0.9 at 3.0 MeV. This means that this reaction can be used as a beam polarimeter at energies greater than 3.0 MeV. Fig. 4 shows one calculation of the polarization asymmetry in the d(γ,n) neutrons at a scattering angle of 90° [5].

Fig. 5 shows one calculation of the differential cross section at a scattering angle of 90° averaged over the azimuthal angle [5]. This differential cross section is the same as what would be expected when using an unpolarized or circularly polarized gamma-ray beam. The cross section peaks at approximately 4.5 MeV, but it is

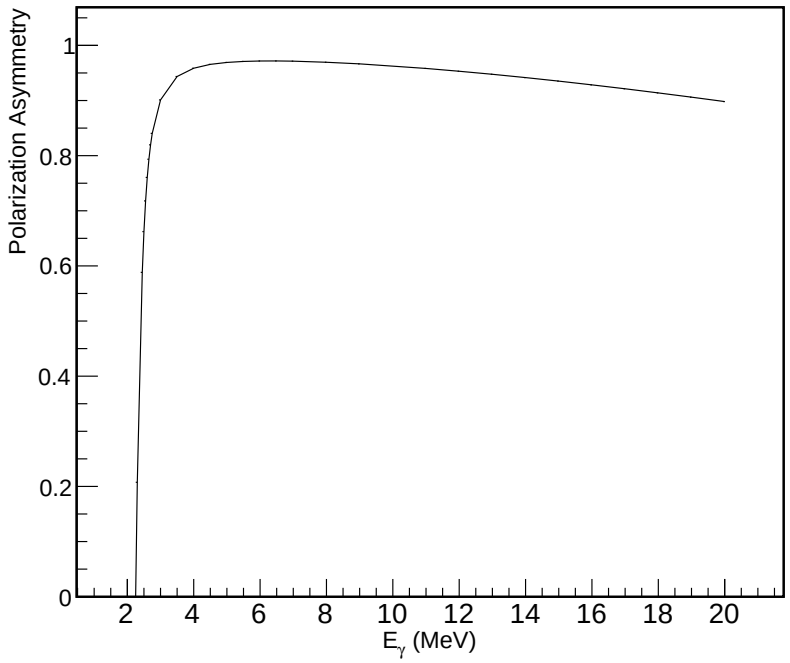

Fig. 4 – A theoretical calculation of the polarization asymmetry using data from Arenhovel [5].

still large even up to 20 MeV. Calculated and measured polarization asymmetries and cross sections for this reaction are in excellent agreement, so we expect systematic uncertainties of the order of a few percent.

The measurement system consists of a deuterium target and an array of three or four neutron detectors at 90° with respect to the beam direction, with two detectors in the plane of the beam polarization, and two detectors perpendicular to this plane. Lithium glass detectors are used in the lower beam energy range from 2.5 to 4 MeV, and NE-213 based detectors are used in the higher energy range from 4 to 20 MeV. The target will consist of D_2O (heavy water) contained in a thin-walled plastic cylinder.

B. Fission chamber

A fission chamber is an ionization chamber with fissionable material deposited on one of the electrodes. Fission chambers are ideal instruments for absolute photon flux measurements as they are simple devices, almost 100% efficient and based on very well-known photo-fission cross sections.

The most studied photo-fission reaction rates are for ^{235}U, ^{238}U, and ^{239}Pu.

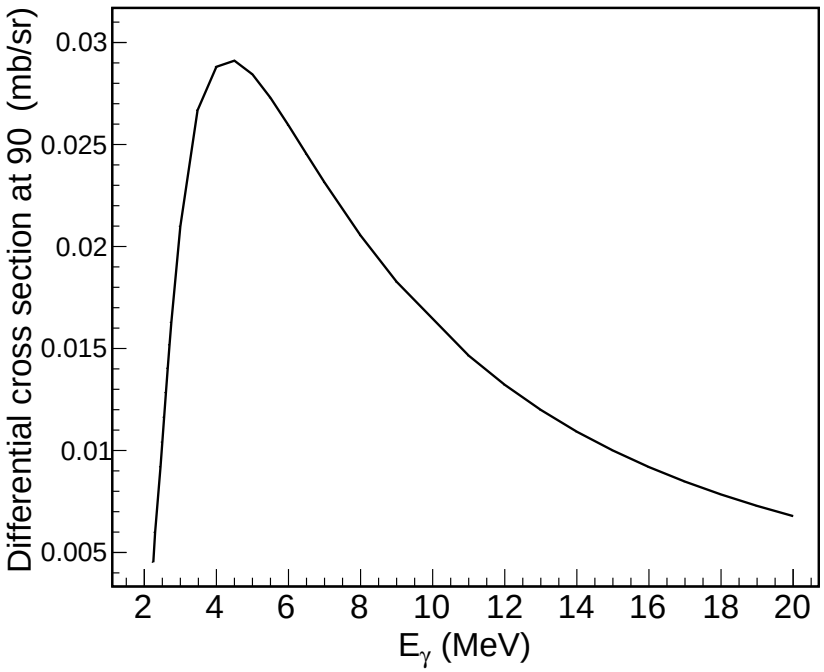

Fig. 5 – A theoretical calculation of the differential cross section at 90° using data from Arenhovel [5].

The cross sections for these isotopes are significant above 5 MeV as shown in Fig. 6.

3.2.3. Gamma beam spatial distribution

An additional CCD camera/flat panel detector system is needed at a position downstream from the experiments to monitor the alignment of the beam line, experimental target and its collimators with the photon beam, as well as monitoring the beam during the experiment.

The principle of operation of the system to be employed is the same as that used at HIγS [7] and briefly described in the EuroGammaS proposal [3]: a CCD camera collects through a mirror the light produced in a scintillator placed in beam.

Because of the high intensity of the beam, a relatively thin scintillator (1–2 mm) will generate enough light to image the gamma beam spot at a microbunch level with very high position accuracy. To allow image collection at microbunch level, a fast CCD camera with externally triggered exposure time will be needed. The design requirements are sub-mm spatial resolution and high contrast sensitivity.

The high-resolution gamma camera (based on a CCD) will also be employed in the prototyping of a 2D-detection system for cone-beam computed tomography

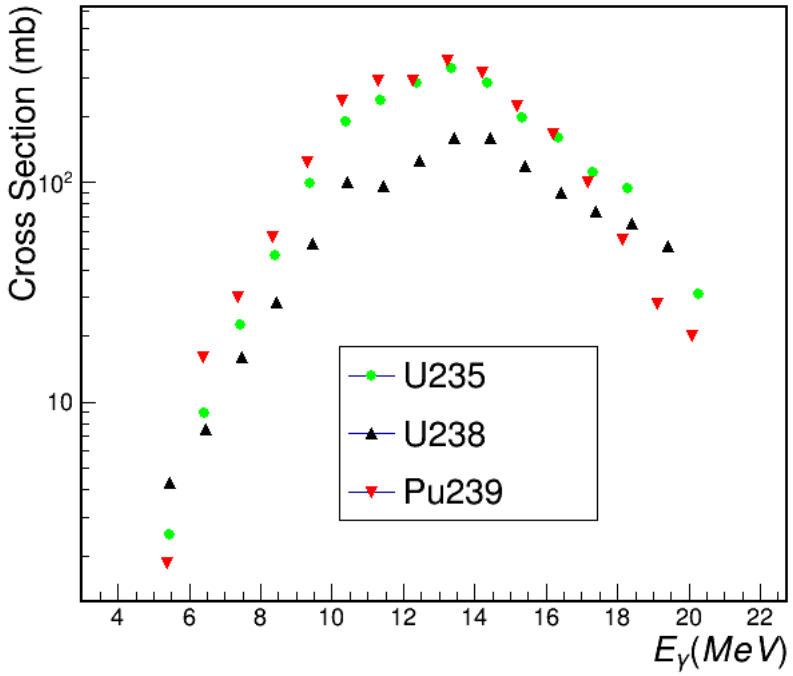

Fig. 6 – Photofission reaction rates for ^{235}U, ^{238}U, and ^{239}Pu based on cross section taken from Evaluated Nuclear Data File ENDF/B-VII.1.

(CT). The CT is the subject of another TDR, GBS-TDR5.2 - Gamma Beam Industrial Applications at ELI-NP, that exploits the unique characteristics of the gamma beam for industrial applications.

3.2.4. Gamma beam time structure

The time structure of the gamma beam at ELI-NP is shown in Fig. 7.

When the gamma beam interacts with a thick slab of material a significant fraction of the radiation is either Compton scattered or generates 511 keV photons (via electron-positron pair generation). The time structure of these events follows the time structure of the beam provided that a fast detector system is placed around the material.

An ideal option for this type of beam monitor would be to place the detector near one of the major beam-matter interaction points. A small (5×5 cm^2) detector based on a fast plastic scintillator or $LaBr_3$ will be used for monitoring the time structure of the beam in both low-energy and high-energy experimental areas. These detectors have a $1/e$ decay time of about 16 ns or less, and may be able to count the

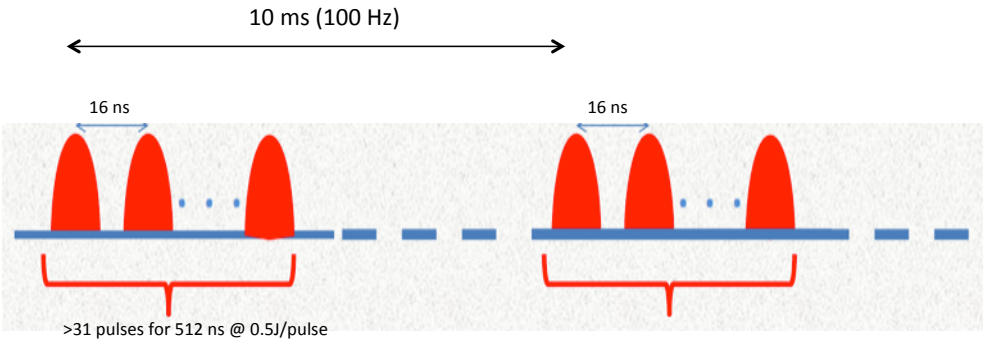

Fig. 7 – A schematic view of the gamma beam time structure.

microbunches in the ELI-NP beam.

3.2.5. Gamma beam polarization

Many proposed experiments at ELI-NP rely on accurate knowledge of the linear polarization of the gamma-ray beam. We are proposing three techniques to determine the beam polarization. One method measures the angular distribution of the neutrons from the d(γ,n) reaction. The other two methods measure photons, either Compton scattered or emitted by Nuclear Resonance Fluorescence (NRF). The use of the d(γ,n) reaction has significant advantages over the NRF technique, but it can only be used above approximately 2.5 MeV. Measurement of Compton scattered photons could be employed at energies below 3.5 MeV as a continuous-energy method for polarization monitoring.

A. The d(γ,n)p intensity monitor and polarimeter

Please see section 3.2.2. for a detailed description.

B. The NRF polarimeter

Linear polarization of the ELI-NP beam can be monitored using the technique of Nuclear Resonance Fluorescence (NRF). A device based on NRF is very sensitive to the beam polarization, but can only be used at specific gamma beam energies corresponding to the selected NRF lines.

In Nuclear Resonance Fluorescence, a gamma ray is absorbed by a nucleus and the nucleus is excited to a particular resonant state. The nucleus then decays from this state back to the ground state by emitting a gamma-ray of approximately the same energy as the incident gamma ray. The angular distribution of the emitted gamma rays depends on several factors: the spins of the ground state and of the excited state, the multipolarity and electric or magnetic character of the transitions,

and the fractional linear polarization of the beam. The sensitivity to measuring the beam polarization is maximized by using a pure E1 or M1 transition on a nucleus with a ground state spin of 0^+. For pure E1 transitions on 0^+ ground state nuclei, there will be no NRF gamma rays emitted at a scattering angle of 90° in the plane of beam polarization. Furthermore, there will be a maximum in the NRF yield at a scattering angle of 90° perpendicular to the plane of beam polarization. Therefore, the linear beam polarization can be determined by measuring the NRF yield at a scattering angle of 90° in and perpendicular to the plane of beam polarization. For M1 transitions, there will be a maximum at a scattering angle of 90° in the plane of beam polarization, and no NRF yield at this scattering angle perpendicular to the plane of beam polarization.

We propose to use the CLOVER detectors from the ELIADE detector array (GBS-TDR1: Nuclear Resonance Fluorescence) to check the beam polarization. Two detectors in the plane of beam polarization, and two perpendicular to this plane are needed to measure the asymmetry in the yields of the NRF lines from E1 or M1 transitions in spin-0 nuclei.

Several candidates for targets have been identified based on the strength of the transition and the availability of the material. The first target to use for the start-up phase of ELI-NP is ^{232}Th. This nucleus has a strong M1 line at 2.043 MeV with an integrated cross section of 46 eV·b [8]. We are proposing initially to use the NRF technique for beam energies below 2.5 MeV. Once energies above 3.5 MeV are achieved, additional promising candidates for NRF include lines in ^{12}C, ^{28}Si, ^{32}S, ^{56}Fe, and ^{208}Pb.

C. The Compton scatterer

The quantum mechanical Klein-Nishina differential cross section for polarized photons is:

$$\frac{d\sigma_{pol}(\vartheta,\phi)}{d\Omega} = \frac{1}{2} r_0^2 \left(\frac{E'_\gamma}{E_\gamma}\right)^2 \left[\frac{E'_\gamma}{E_\gamma} + \frac{E_\gamma}{E'_\gamma} - 2\sin^2\vartheta\cos^2\phi\right] \tag{3}$$

The angle between the two polarization vectors is ϑ, while the scattering angle is ϕ. E_γ is the energy of the incoming gamma ray and E'_γ is the energy of the Compton scattered gamma.

We propose a system based on four HPGe detectors placed at a moderate scattering angle around 30 and azimuthal angles of 0°, 90°, 180°, and 270°. This system could be used to monitor not only the polarization of the gamma beam but also the beam energy and the relative intensity.

4. TECHNICAL PROPOSAL

4.1. GAMMA BEAM DELIVERY

All the gamma beam transport will have to take place in vacuum because the high intensity of photons will lead to the creation of forward scattered clouds of electrons and photons which will otherwise impact the subsequent experimental targets and beam diagnostics.

The vacuum pipe will be modular, allowing the removal of each 1.5 m segment for the placement of experimental apparatus. The pumping stations will be distributed according to their pumping power, making vacuum connections between sections of pipe where that is necessary.

4.2. COLLIMATORS

Collimators will be placed before each experimental apparatus to reduce the background from scattering inside the transport pipe.

Five sets of collimators of different diameters will be machined. The design of the collimators and their support structure will allow their interchange if needed. Tungsten alloys are considered as lead substitutes for collimators, but their hardness and high melting points makes them difficult to be machined or cast. Direct laser metal sintering has been successfully applied to manufacture collimators of pure tungsten up to 10 cm thick.

4.3. BEAM DUMPS

The beam dumps for the gamma-ray beam should ensure complete absorption of the gamma beam and its reaction products and minimize the back scattering of radiation into the experimental vault. Two different types of beam dumps have to be built: one for the low-energy gamma-ray beams up to 3.5 MeV and another one for the high-energy gamma-ray beams up to 19.5 MeV. Fig. 8 shows the location of the low-energy (LE) and high-energy (HE) beam dumps in E8 vault.

Radioprotection calculations were performed for the beam dump in E8 with the MCNP code [9]. A schematic view of the beam dump as implemented in MCNP is show in Fig. 9. Gamma rays and neutrons were considered. A beam dump integrated in the vault wall, composed of lead, paraffin, and cadmium met the radiological criteria.

Five smaller beam dumps for the already collimated beam are going to be built at the exit from each of the experimental areas to stop the beam and ensure safety of work in the downstream rooms.

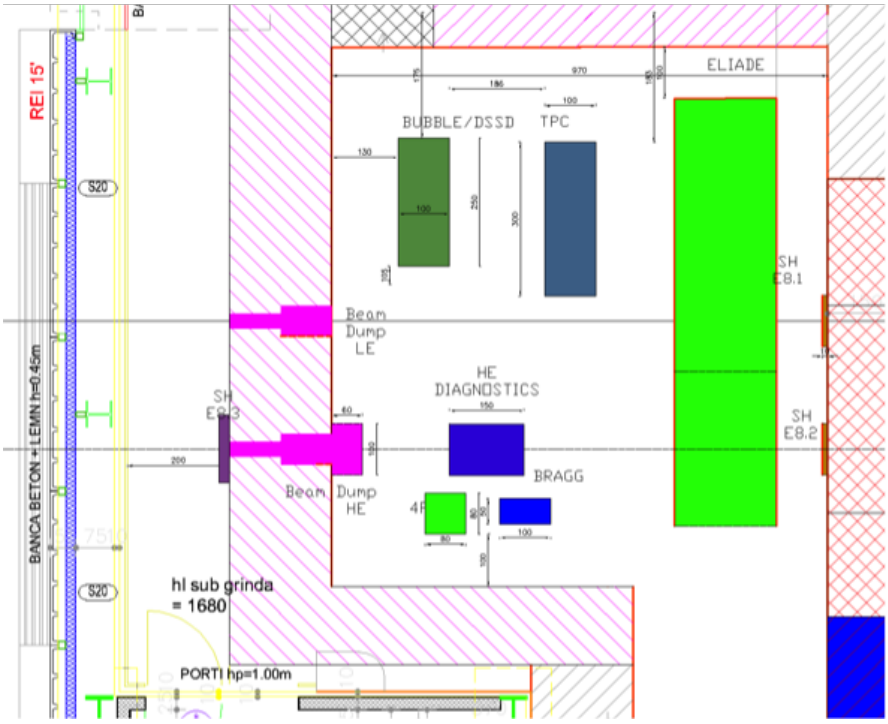

Fig. 8 – Illustration of the beam dumps in the E8 vault. The beam dumps are embedded in the external concrete vault on the left.

4.3.1. Shielding

Lead shielding walls will be placed before each experimental setup to minimize downstream scattered background. A number of six walls are envisioned, each of 5-cm thickness and an area of 1 m^2. The design of the lead shielding walls will be modular to allow for easy dismantling and moving along the beamline. A combination of collimator and shielding wall is envisioned.

4.3.2. Secondary electrons removal

Dipole magnets shall be placed around the beam line to remove secondary electrons originating at the collimators. No special power supplies are need for these magnets as magnetic field stability is not an issue with these magnets. A total number of 10 sweeper magnets are proposed to be placed on the beam transport line.

4.3.3. Alignment system

The total length of the low-energy beam transport line from the photon generation point to the low-energy dump in room E8 is 80 m. The high-energy beam

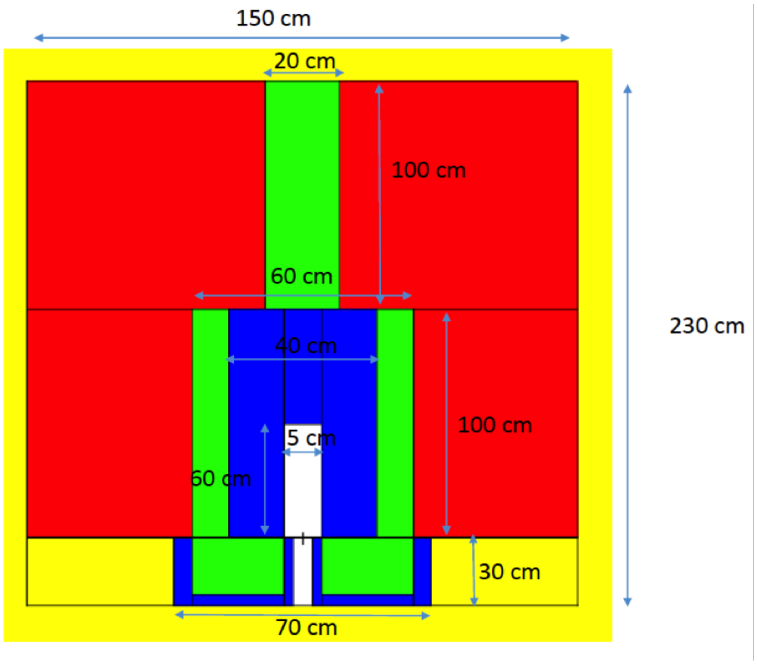

Fig. 9 – Drawing of the high-energy beam dump as implemented in MCNP (green is for Pb, orange is for paraffin, red is the concrete wall, yellow is air).

transport line measures 30 m from the photon generation point to the high-energy dump in E8.

A laser positioned behind the photon generation point will be directed along the beam transport line mimicking the photon beam path. The laser will be positioned in air and it must be rigidly mounted to the floor if it is to be used as a reference standard. The laser beam enters the vacuum through an optical window. The requirements for the laser system are: i) auto-levelling function with blocking function, ii) rotation in the horizontal plane, iii) vertical height adjustment.

Use of this tool will simplify alignment of the beam transport components and of the experimental stations which could be completed before photon beam time begins.

4.4. GAMMA BEAM DIAGNOSTICS

4.4.1. Gamma beam energy spread

The gamma-ray beam energy spectrum will be determined using two different type of detectors depending on the beam energy. For beam energies below 8 MeV, a large volume HPGe detector will be used to directly measure the beam energy

spectrum. The HPGe detector will be placed directly in an attenuated beam. The detector should be placed slightly off of the beam axis to avoid directly hitting the cold finger, which would reduce the resolution and efficiency. An HPGe detector with a relative efficiency of 120–150% should be adequate for this purpose. To avoid significant pile-up effects in the detector, the flux incident on the detector should be kept to approximately 10 Hz. A 5-cm thick and 25-cm long NaI anti-Compton shield will be used to reject Compton scattered events in the detector.

The HPGe waveform will be recorded using a digitizer. A 14-bit, 500 MHz digitizer should be used for the HPGe and NaI shield to take advantage of the intrinsic resolution of the HPGe. One input of the digitizer should be reserved for the accelerator signal and another channel should be used to record which attenuators are in the beam. A bit pattern can be used for the attenuators.

The attenuator system will be located in the Gamma Source Room and is placed on a platform that can be removed from the beam. Although the attenuator will be stopping the beam completely, it cannot substitute the upstream beam dump as the attenuator will be creating a high background in the Gamma Source Room. The attenuator system consists of (natural) copper cylinders that can be placed in the beam individually or in any multiple combinations desired. The attenuators are remotely controlled by the experimenter. A schematic of the system is shown in Fig. 10. The length of each attenuator should be known to 1%. These lengths were chosen so that cylinders will attenuate the beam by a different factor, knowing that at E_γ = 5 MeV, 8 cm of copper will reduce the beam by a factor of 10.

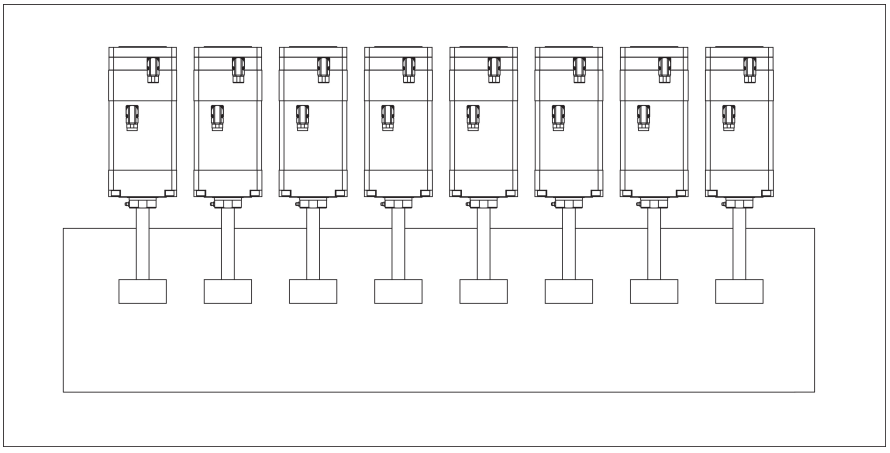

Fig. 10 – Schematic drawing of the attenuator system with eight blocks moved by pneumatic actuators.

The attenuator system could be used as an intensity monitor if the attenuation factor as a function of gamma-ray energy of each Cu cylinder is known. Attenuation

factors for an 8-cm cylinder have been measured at HIγS, see Fig. 13, for several gamma-ray energies and compared with theoretical attenuation curves. For beam energies above 8 MeV, a 7.6-cm diameter and 10-cm long $LaBr_3$ detector will be used to characterize the beam energy spectrum. These detectors have a $1/e$ decay time of about 16 ns, and may be able to count the microbunches in the ELI-NP beams, which occur every 16 ns, with 32 bunches every 10 msec giving 3200 pulses per second. This would only require approximately 50 cm of Cu to attenuate the beam to 10^3 Hz.

Fig. 11 shows the expected ratio of the number of pileup events to the total number of events as a function of the amount of copper attenuation. The flux was assumed to be 8.3×10^6 per macrobunch, and it was assumed that the $LaBr_3$ detector could resolve neighboring microbunches. The HPGe detector can only resolve the macrobunches. A beam energy of 8 MeV was assumed since the attenuation factor for copper is the lowest at this energy; this energy represents the scenario where the shielding is the least effective. At other beam energies, less shielding will be adequate. Absolute detection efficiencies of 100% were assumed.

We recommend that the fraction of pile-up events be kept below 0.1. This requires approximately 65 cm of copper attenuation for the HPGe detector, and approximately 50 cm of copper attenuation for the $LaBr_3$ detector. We recommend that a variety of different sized copper pieces be machined to high precision to act as attenuators. The various thicknesses we suggest are: 1.5 cm, 2.5 cm, 5 cm, 10 cm.

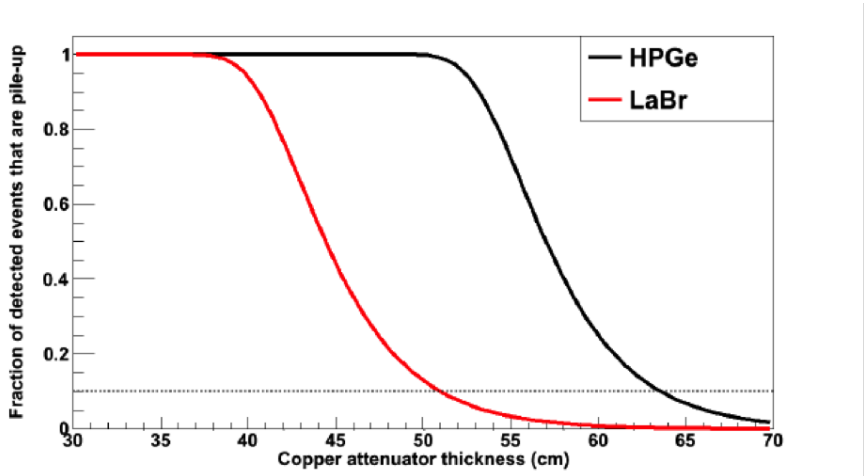

Fig. 11 – The fraction of detected events that are pile-up is shown as a function of the thickness of copper attenuators, assuming a beam intensity of 8.3×10^6 gammas per macrobunch and that the $LaBr_3$ detector can resolve individual microbunches.

The precise attenuation factor of each copper block will be measured directly

using the gamma-ray beam and the $LaBr_3$ detector during the commissioning phase of operations by rapidly and repeatedly inserting and removing each block from the beam. Assuming the beam is stable over the short term, the attenuation factor of the block can be determined by the ratio of gamma rays incident on the in-beam $LaBr_3$ detector when the block is in the beam and when it is removed.

4.4.2. Gamma beam flux

A. The d(γ,n)p intensity monitor and polarimeter.

A system based on d(γ,n) reaction has been successfully used for many years at HIγS for intensity and polarization measurements. Tests have been performed recently at HIγS to assess the prospects of using the d(γ,n) reaction at ELI-NP.

Four liquid scintillator detectors were used to detect the outgoing neutrons from the d(γ,n) reaction for gamma beam energies above 4 MeV. The liquid scintillator was BC-501A. The active volume of the detectors was 12.5 cm in diameter and 5-cm thick. Two detectors were placed in the horizontal plane at a scattering angle of 90° (one to the left of the beam and another to the right), and the other two detectors were placed in the vertical plane at a scattering angle of 90° (one above the beam and the other below the beam). The target was heavy water (D_2O) in a 5.03-cm long and 3.18 cm diameter plastic cell. The detectors were placed approximately 71 cm from the target position.

Measurements were carried out at five different energies: 5.0, 6.1, 7.0, 15.0, and 20.0 MeV [10]. The first measurement at each energy was performed using a 100% circularly polarized gamma-ray beam. This measurement is used to correct for any instrumental asymmetries, such as differences in detector distances or detection efficiencies. Measurements with the linearly polarized beam are taken after the circularly polarized beam measurements.

The measured polarization asymmetry varies depending on the location of the low energy cut shown in Fig. 12 (leftmost red line). There are two causes for this effect: finite size corrections and multiple scattering. To account for these effects, a full Monte Carlo simulation of the target and detectors was performed using GEANT4 [11]. Several systematic uncertainties were investigated to assess the stability and reliability of this technique. The dominant systematic uncertainty is from the uncertainty on the theoretical predictions of Arenhovel [5], which we have taken to be approximately 1%.

There were no significant corrections to the data required for the beam intensity measurements in this case since, unlike the case of the asymmetry measurements, the entire neutron peak was summed. There was no systematic uncertainty on the low energy cut shown in Fig. 12 in this case, since the entire neutron peak was summed.

This technique can be reliably used at ELI-NP above 4 MeV. The primary difference in performing experiments at HIγS versus ELI-NP is the time structure of the

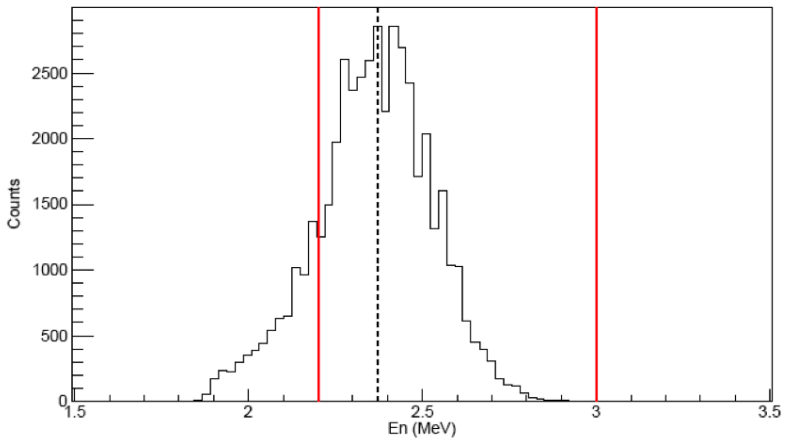

Fig. 12 – Neutron energies at a beam energy of 7.0 MeV. The red lines indicate the summing window for the polarization asymmetry measurement.

beam. Backgrounds in time with the beam can be significantly reduced by shielding the detectors with thin pieces of lead. The only major consideration is that the count rate must be limited in order to ensure good Pulse Shape Discrimination (PSD) performance. With microbunches every 16 ns, we estimate that there should be a gap of at least 5 microbunches between detector hits for good PSD performance. A conservative estimate would be to run the detectors at an average beam-related trigger rate of approximately 200 Hz. The neutron detectors will be made of NE213-type liquid scintillator. These detectors have been well studied and characterized at facilities around the world. They will be 12.7 cm in diameter and they will be placed approximately 50 cm from the target. This scintillator material has excellent (PSD) properties, which is essential to distinguish neutron from gamma events. If the target is made to be 3-cm thick, a beam intensity of 10^8 γ/s will result in a counting rate of about 10 counts per second. This means that one can obtain 1.5% statistics in a 10 minute run.

The four neutron detectors which will be used at energies below 4 MeV will be made of Li-6 doped glass. These will be about 5 cm in diameter and 1-cm thick. The virtue of these detectors is that they can count very low energy neutrons and are not subject to the threshold problems associated with fast plastic scintillators. In addition, their efficiencies are well known for neutron energies below 1 MeV.

Results from tests performed at HIγS below 4 MeV showed excellent agreement between the measured and expected asymmetries. A full simulation of multiple scattering effects using GEANT4 is required for accurate beam intensity measurements at these energies. A similar 200 Hz trigger rate is advised for the system to be

implemented at ELI-NP.

We propose placing the detectors as shown in Fig. 13. The in-plane and out-of-plane detectors will show a significant difference in counts, due to the large beam polarization and large polarization asymmetry in the d(γ,n) reaction. The detector located at 45° with respect to the plane of beam polarization will be used to measure any misalignment in the plane of beam polarization or any component of circular polarization. The polarization plane should be frequently rotated by 90° to account for any systematic effects.

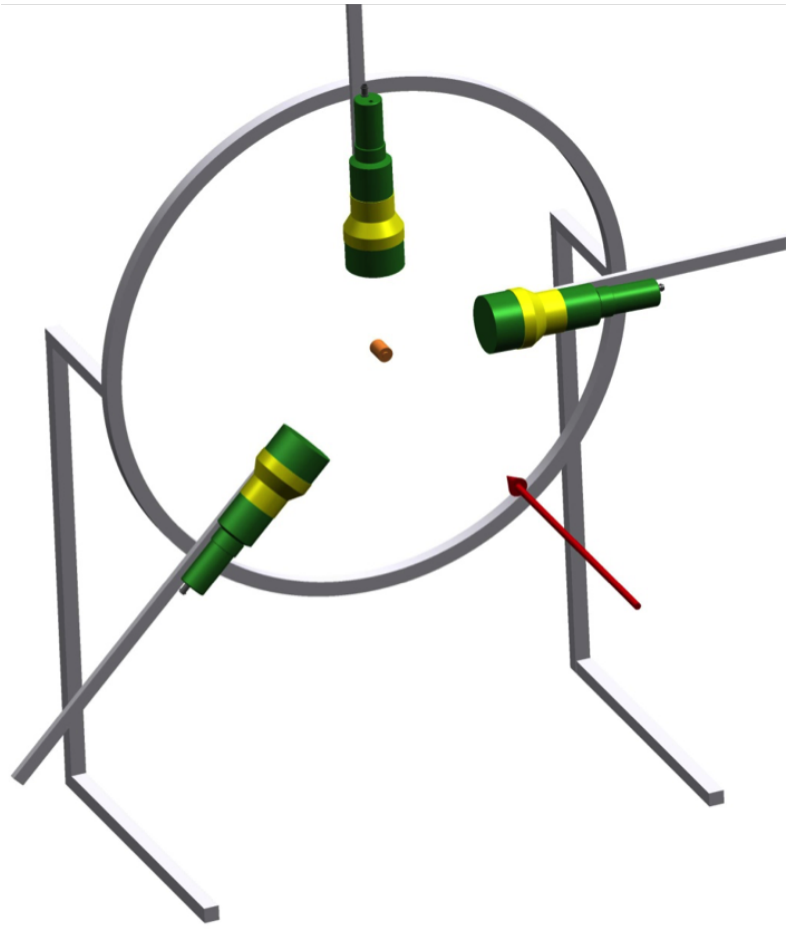

Fig. 13 – A schematic view of the three neutron detectors in the d(γ,n) polarimeter design.

The waveforms from the liquid scintillator detectors should be digitized with a 12 or 14-bit, 500 MHz digitizer. Good timing will be essential to identifying neutrons

from d(γ,n) based on their time-of-flight and to correctly discriminate neutrons from gamma rays using PSD. Two inputs on the digitizer should be reserved for accelerator inputs: an input for the beam polarization (horizontal or vertical) and an input for the timing of the beam bursts for use in neutron time of flight measurements

If possible, the same detector support structure should also be used for the Compton scattering system. It should be flexible enough to be able to mount either HPGe, NE-213, or Li-glass detectors. The ability to adjust the distance between the target and each detector from 25 cm to 1 m would be highly preferred. Additionally, in this support structure, the amount of material around the detectors and target should be minimized so that the effects of multiple scattering are kept as small as possible. Beam intensity measurements with this device should be accurate at the 5% level since the cross sections for this reaction and the detector efficiencies are well known.

B. Fission chamber

The current output of a parallel plate ionization chamber is directly proportional to the total number of electrons between the electrodes at a given moment, the drift velocity of the electrons, and the distance between the electrodes:

A distance of 3 mm provides a good current ratio of 10:1 between fission fragments moving along the electric field and 5.5 MeV alpha particles moving in the perpendicular direction. At δ U = 500 V for P-10 gas (90%Ar+10%CO_2), the drift velocity is 5×10^6 cm/s which gives a 50 ns pulse width.

The fission chamber will be used for absolute photon flux measurements in the high-energy experimental halls (E7, E8). The sketch of the fission chamber is shown in Fig 14.

The fissionable material (^{235}U, ^{238}U, ^{239}Pu) is deposited with an active spot of 10 mm on a 0.2 mm thick, 20 mm diameter aluminum or stainless steel backing. The chamber is constructed of stainless steel with a thickness of 0.2 mm. The design geometry minimizes the amount of material in the gamma beam and moves all the massive parts away from the interaction point. The chamber is filled with P-10 gas up to 1.2 bar. Should be leak free, easy to fill and maintain the desired pressure over long periods of time. Alternatively, it can be fitted with a pressure monitor system and automatic gas top-up.

The fission detection efficiency of similar designs was reported [12] to be greater than 98.5%. The detection efficiency of the chamber should be checked with a ^{252}Cf source in the same configuration as the photofission target. The choice of backing material is based on the actinide deposition method. The total activity of the actinide layer, the derived mass and areal density can be determined by low-geometry alpha-particle counting to better than 1% uncertainty [13].

The count rates for ^{235}U, ^{238}U, ^{239}Pu are shown in Fig 15. The analytical calculations are based on 100 fissions/s recorded by the fission chamber with ^{235}U

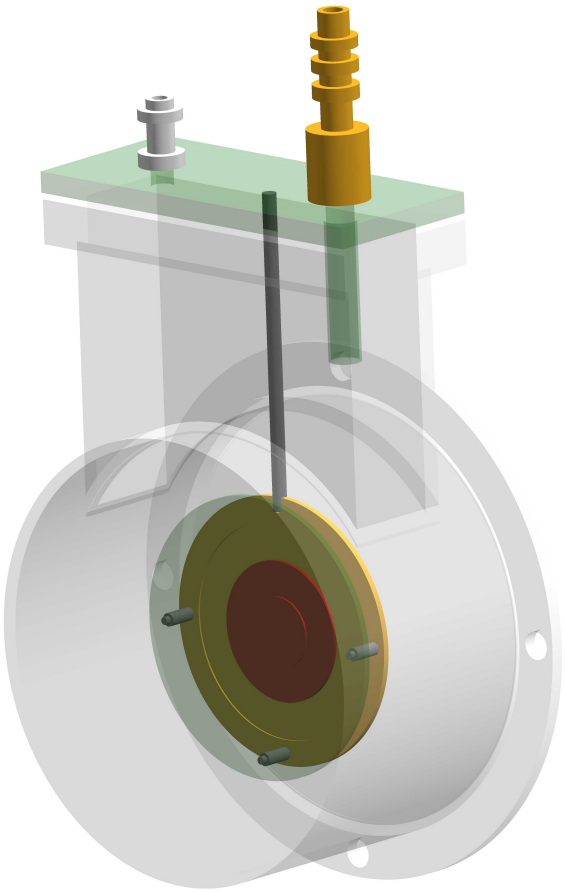

Fig. 14 – Fission chamber general view. The actinide deposit is visible in red on the cathode. The chamber has circular central configuration for easy centering, with signal and gas connectors located outside the beamline.

at maximum cross section (330 mb at 14 MeV). The resulting actinide deposit is 200 μg/cm^2. This rate gives a 1% uncertainty in under two minutes between 10 and 16 MeV and around 20 minutes in the remaining range. We are exploring the possibility of operating the fission chamber at higher detection rates in pulsed mode or even in current mode.

Beam intensity measurements with this device should be accurate at the 5% level since the cross sections for this reaction are very well known [14] and the instrument efficiency is almost 100%.

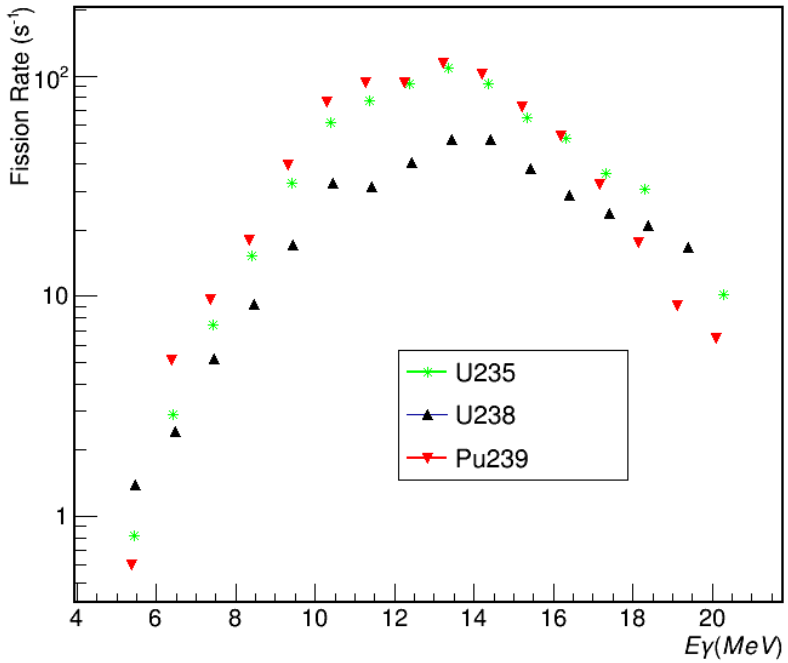

Fig. 15 – Photofission reaction rates for three actinides based on a 200 μg/cm^2 deposit.

4.4.3. Gamma beam spatial distribution

The gamma beam spatial distribution system utilizes a CCD camera [7] to collect the light produced in a scintillator placed in the beam by means of a mirror (see Fig. 16). The system is designed to be mobile and could be moved to different experimental areas. Specific ports will be constructed in E2, E7 and E8 for rapid deployment of the gamma beam spatial distribution system.

Because of the high intensity of the beam, a relatively thin scintillator (2 mm) will generate enough light to image the gamma beam spot at a microbunch level with very high position accuracy. To allow image collection at microbunch level, a fast CCD camera with externally triggered exposure time will be needed. The camera will be placed outside vacuum in a special mount which ensures position reproducibility and easy removal. The scintillator and the mirror will be housed in a light-tight box inside the beam transport pipe. Several options are considered for the mirror, either having a very thin 3M film in the beam or having a retractable mechanism which could remove the mirror from the beam when the system is not used,

Several commonly used scintillators are considered for the scintillator screen.

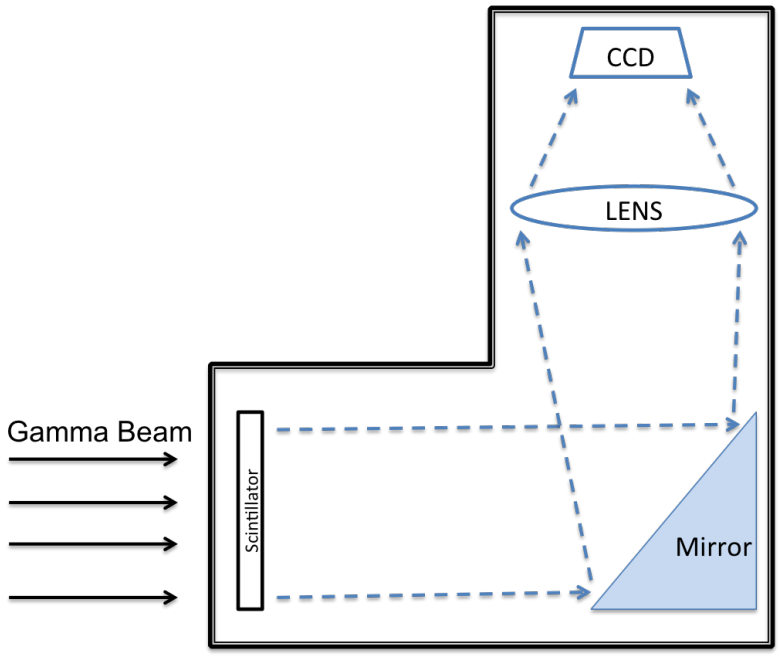

Fig. 16 – Diagram of the CCD-based spatial distribution monitor. Gamma beam enters from the left, scintillation light is reflected by a mirror into the CCD camera.

The ideal scintillator screen should have a high density, a short decay time, high light yield and be radiation resistant. The properties of several commonly used scintillators are presented in Table 2. $LaBr_3$ has the shortest decay time and high light yield but it is hygroscopic which requires special packaging materials. BGO and LSO are a viable alternative as they are not hygroscopic and have high density. The light yield could be increased by coating the scintillators with a thin layer of Pb.

Table 2

Characteristics of several common scintillators.

Detector	NaI(Tl)	CsI(Tl)	BGO	LSO	$LaBr_3$
Density (g/cm3)	3.67	4.51	7.13	7.35	5.29
L_{rad} (cm)	2.59	1.85	1.12	0.88	2.1
Decay time (ns)	230	1000	300	40	16
Light yield (photons/keV)	38	54	8–10	25	63
Luminescence (nm)	410	530	480	420	380
Hygroscopic	Yes	Slightly	No	No	Yes

We calculate the probability of interaction and the average deposited energy in

Table 3

The probability of interaction and the average deposited energy of photons of 3.5 MeV in a scintillator converter.

	BGO	BGO	LSO	LSO	CsI(Tl)	CsI(Tl)
Thickness	ϵ	δE_{ave} (MeV)	ϵ	δE_{ave} (MeV)	ϵ	δE_{ave} (MeV)
0.5	0.014	0.314	0.015	0.31	0.008	0.17
1	0.027	0.582	0.03	0.59	0.016	0.33
2	0.054	1.038	0.06	1.05	0.032	0.64
4	0.101	1.628	0.11	1.63	0.063	1.13

scintillator convertors of different thickness for gamma rays of 3.5 MeV (see Table 3 and Fig. 17). The number of scintillation photons increases dramatically for LSO and CsI(Tl) as the thickness increases. A compromise has to be found between the number of scintillation photons and spatial resolution which degrades as the convertor thickness increases.

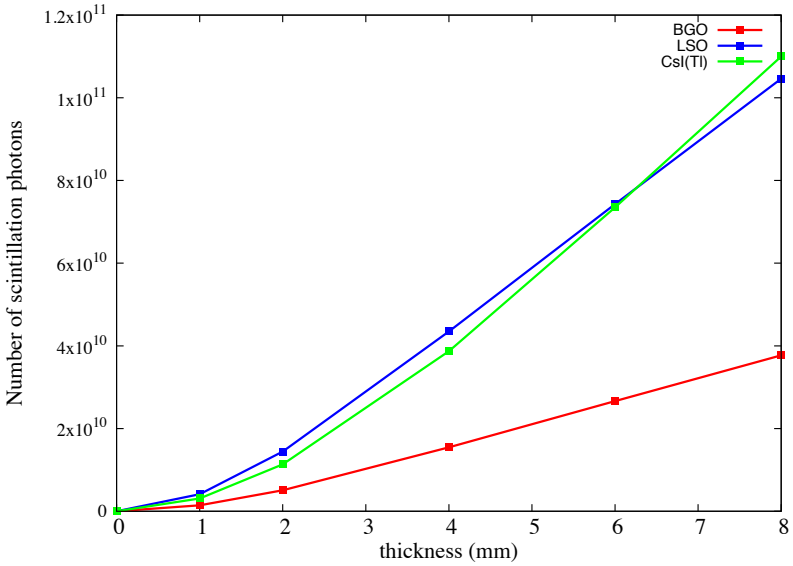

Fig. 17 – The number of the scintillation photons as a function of the converter thickness. The simulations were done using 10^7 incident photons of 3.5 MeV energy.

4.4.4. Gamma beam polarization

A. The d(γ,n)p intensity monitor and polarimeter.
Please see section 4.2.2. for a detailed description.

B. The NRF polarimeter.

A recent experiment was carried out at the HIγS to test the feasibility of using NRF on ^{232}Th as a beam polarimeter. The experimental setup consisted of two 60% HPGe detectors placed at a scattering angle of 90° relative to the beam direction. One HPGe detector was placed in the horizontal plane at 90° and another HPGe detector in the vertical plane at 90°. Both detectors were approximately 12.5 cm away from the thorium foil. Two different ^{232}Th targets were used: a 1-mm thick disk of ^{232}Th of 2.54 cm diameter, and a 2-mm thick disk of ^{232}Th of 1 cm diameter. The beam was collimated using a 1.9 cm diameter collimator for these runs. The target thickness was varied during the experiment by using either the 1-mm thick target or the two targets combined to make a total target thickness of 3 mm.

The data described here were taken with 3 hours of beam time, with the 100% linearly polarized gamma-ray beam at a beam intensity of approximately 9×10^6 γ/s on target and a beam energy spread of approximately 4.2%. Fig. 18 shows results of the measured spectra for the in-plane (horizontal) and out-of-plane (vertical) HPGes. The spectra show significant peak at 2043 keV in the in-plane detector and no peak in the out-of-plane detector.

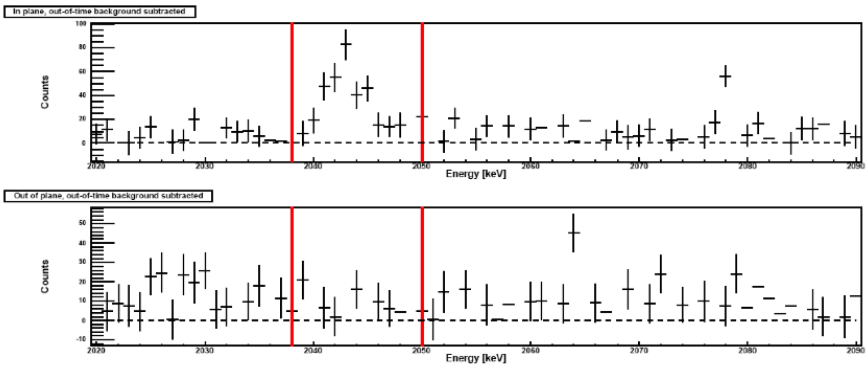

Fig. 18 – Gamma-ray peak visible at 2043 kev in the in-plane HPGe (top). No peak visible in the out-of-plane detector (bottom)

The measured asymmetry for this run is 0.84±0.17. In this analysis, the asymmetry is determined only by summing the yield within the red summing window. Fitting methods could improve the robustness of extracting the asymmetry. The primary correction to these measured asymmetries is due to the finite size of the de-

tectors, the beam spot, and the target. A Monte Carlo simulation was developed to determine the size of this correction. This relatively simple finite size correction predicts an observed polarization asymmetry of 0.92 for a true polarization asymmetry of 1.0.

The most significant challenge to running this experiment at ELI-NP will be the effect of pile-up due to the beam time structure. The beam time structure will allow us to easily subtract out detected gamma rays that are not related to the beam. Unfortunately, any gamma rays arriving in the HPGe within the same macropulse will pile up in the HPGe. We have simulated the impact of pile-up on the measured spectra at different count rates. At a count rate of 1 Hz, the effect of pile-up is negligible and a significant asymmetry is present. However, the asymmetry smoothly decreases as the count rate increases. This effect is caused by an increase in background in the out-of-plane detector from the increased pile-up. Using the segmented CLOVER detectors from the ELIADE array we expect to sustain count rates around 100 Hz. We estimated that a 5% polarization measurement at ELI-NP with the detector count rate limited to 100 Hz would take less than an hour of continuous running.

C. The Compton scatterer.

We propose a system based on measuring the Compton scatted gamma rays to determine the gamma beam polarization and beam energy. The Klein-Nishina formula predicts a difference in the cross section measured in the polarization plane and in a plane perpendicular to the polarization plane.

Let's assume a linearly polarized gamma beam with an energy of 2.5 MeV. We can calculate a cross section of 25 mb for the Compton scattered photons at a polar angle of 30° in the polarization plane and 32 mb in the perpendicular plane (at the same polar angle of 30°). The scatterer is a small Cu cubic block of 1 mm^3. A lead collimator in front of each detector will minimize the spread in energy and thus ensure a good energy resolution measurement. With the detectors at 30 cm from the Cu scatterer and a 6-mm diameter opening of the collimator we would get a rate of 30 Hz in the detectors.

The HPGe waveform will be recorded using a digitizer. A 14-bit, 500 MHz digitizer should be used for the HPGe detectors to take advantage of their intrinsic resolution. One input of the digitizer should be reserved for the accelerator signal and another to record the polarization settings.

4.5. ELECTRONICS AND DAQ

Although the detectors used for the gamma beam diagnostics are different, we propose to keep the types of digitizers to a minimum. A common digitizer will keep costs down and ensure a quicker implementation of acquisition software and analysis

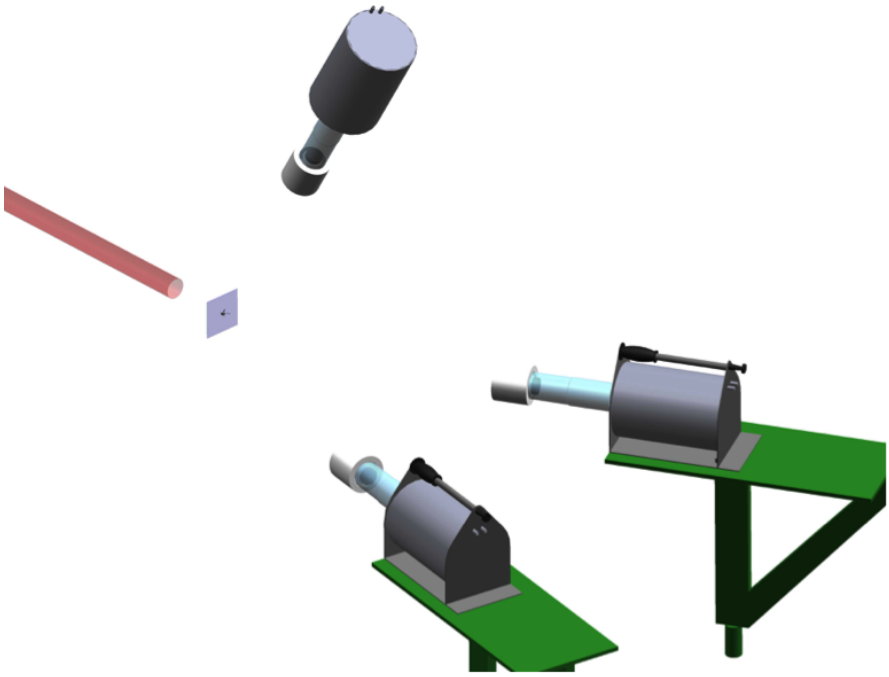

Fig. 19 – A schematic view of the HPGe detectors in the Compton scattering monitor.

routines.

The beam energy measuring system described in section 4.2.1 will use a 14-bit, 500 MHz digitizer for the HPGe and the NaI anti-Compton shield. Five channels are needed to record the detectors waveforms and one channel should be reserved for recording the attenuator configuration. The attenuator will be remotely controlled using specific electronics and communications equipment.

The d(γ,n)p intensity monitor and polarimeter uses three neutron detectors, either NE-213 or Li-glass depending upon the beam energy. Three channels of 12 or 14-bit, 500 MHz digitizers are needed to record the waveforms. One channel should be reserved for recording the beam polarization. Fast bi-polar amplifiers will be needed for the Li-glass detectors.

The fission chamber will need one channel, 12-bit and minimum 250 MHz. One Mesytec MPR-1 preamplifier will be needed for the cathode signal.

One 5$\times$5-cm fast plastic scintillator or $LaBr_3$ detector will be used to monitor the time structure of the beam. One channel of 14-bit, 250 or 500 MHz digitizer should be used.

We require a minimum of 16 digitizer channels for recording the detector waveforms. An additional channel is required for recording the accelerator time structure in case all the digitizers are housed in the same bin.

The monitoring systems will be controlled and the data handled and stored by two separate stations, one in the low-energy area and another in the high energy area. Power crates for the digitizers, computers and data storage will be distributed for each system.

4.6. HV AND LV POWER SUPPLIES

All the detectors used for gamma beam diagnostics require high voltage power. Nine channels of HV are required. Most of the monitoring measurements are very sensitive and require precise control of the high voltage levels.

4.7. LIQUID NITROGEN FILLING SYSTEM

The three HPGe detectors used in the NRF polarimeter are grouped together while the HPGe used for monitoring the energy spread is placed in the back of the E2 experimental hall. Connection of the HPGe detectors to the automatic, centralized LN2 filling system is not practical. Two LN2 Dewar vessels will be used to ensure timely filling of the detectors.

4.8. LAYOUT OF THE EXPERIMENTAL HALL AND LOCATION OF THE GAMMA BEAM DIAGNOSTICS SYSTEMS

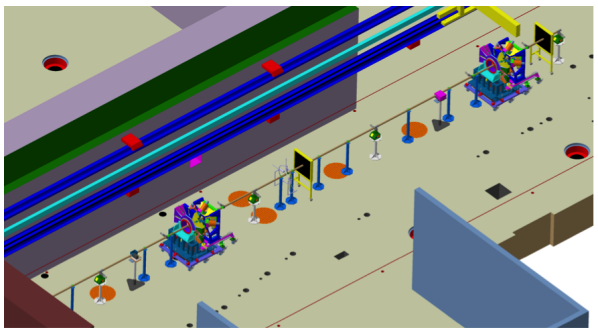

Fig. 20 – Gamma beam delivery and diagnostics systems layout in the low-energy area E2. Two locations of the ELIADE array could be seen together with two shielding walls, pumping stations (green) and CCD camera (pink box)

5. SPECIFIC NEEDS AND UTILITIES, TRANSVERSAL NEEDS

We have identified the following infrastructure needed from ELI-NP to implement the TDR:

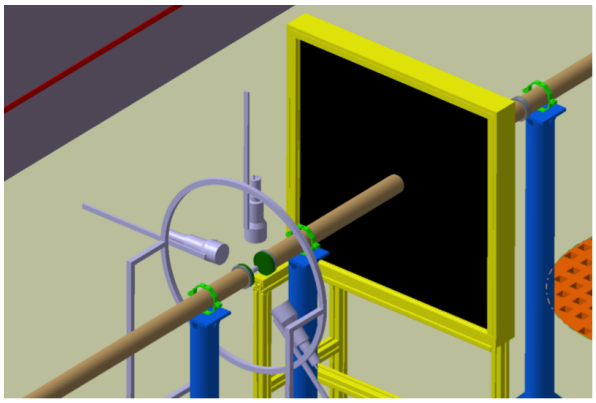

Fig. 21 – Details of the gamma beam delivery and diagnostics systems layout in the E2 area around the d(γ,n) polarization setup.

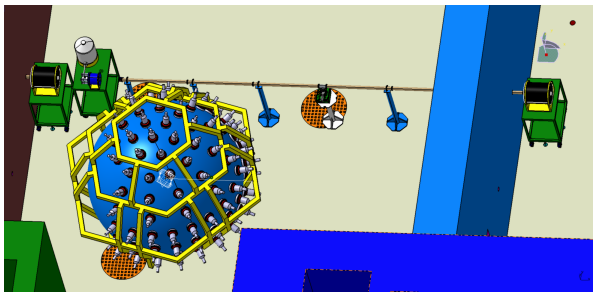

Fig. 22 – Gamma beam delivery and diagnostics systems layout in the low-energy area E7. The location of the energy spread monitoring detector system is shown together with the beam dump (black) and one pumping station (green).

1. Clean power supply lines; clean grounding connections
2. Support in designing and placing the equipment
3. Mechanical and electronic workshop
4. Beam-line support structures
5. High-speed data connection line
6. High-speed storage system

6. SAFETY REQUIREMENTS

The NRF polarimeter and the photo-fission chamber use actinide targets with very limited activity. Mounting of these targets inside the experimental devices

should follow local rules and regulations concerning handling of radioactive materials.

A ^{252}Cf time-tagged fission chamber and standard gamma-ray calibration sources will be used for the characterization of the neutron detectors in the D_2O system.

Pressurized gas containers with flammable gases will be used to for the fission chamber. Leakage monitors should be available in the area where the fission chamber will be located.

7. CONCLUSIONS

The High Brilliance Gamma Beam System of ELI-NP will produce tunable, intense gamma-ray beams with high spectral density, narrow bandwidth, and high degree of polarization starting in 2017. The GBS will be built in two phases with two separate beamlines: the low-energy phase will produce gamma beams up to 3.5 MeV starting in 2017, while the high-energy phase will produce gamma beams up to 19.5 MeV in 2018. The transport of the gamma beam takes place under vacuum. Beam dumps will ensure complete absorption of primary photons and secondary radiation. Several instruments are proposed for monitoring the spectral, temporal, and spatial characteristics of the gamma beam. Details of the beam transport equipment and monitoring instruments together with their layout in the building are presented in the paper.

Acknowledgements. CAU, CM, GS, VI, and ZY were supported by the Project Extreme Light Infrastructure - Nuclear Physics (ELI-NP) - Phase I, a project co-financed by the Romanian Government and European Union through the European Regional Development Fund. The authors would like to acknowledge the help received from the engineering bureau, especially from C. Petcu, B. Tatulea, and E. Udup.

REFERENCES

1. Extreme Light Infrastructure-Nuclear Physics (ELI-NP) White Book
2. F. Albert *et al.*, Phys. Rev ST Accel. Beams **13**, 070704 (2010).
3. O. Adriani *et al.*, Technical Design Report EuroGammaS proposal for the ELI-NP Gamma beam System, arXiv:1407.3669.
4. B.A. Perdue, Measurements of the Absolute Cross Section of the Three-body Photodisintegration of ^{3}He Between E_γ = 11.4 MeV and 14.7 MeV at HI$gamma$S, PhD Thesis, Duke University (2010)
5. H Arenhovel and M Sanzone. Photodisintegration of the Deuteron: A Review of Theory and Experiment. Springer-Verlag, Vienna, 1991.
6. M. A. Blackston *et al.*, Phys. Rev. C **78**, 034003, (2008).
7. C. Sun, Characterizations and Diagnostics of Compton Light Source, PhD Thesis, Duke University (2009).
8. A.S. Adekola, C.T. Angell, S.L. Hammond, A. Hill, C.R. Howell, H.J. Karwowski, J.H. Kelley,

and E. Kwan, Phys. Rev. C **83**, 034615 (2011).
9. MCNP: a general purpose Monte Carlo code for neutron and photon transport, LA-7396-M, Los Alamos National Laboratory, USA.
10. J M Mueller *et al.*, Nucl. Instr. and Meth. in Phys. Res. A **776**, 107 (2015).
11. The GEANT4 Collaboration, Nucl. Instr. and Meth. A **506** (2003) 250, 303.
12. N.V. Kornilov, High Intense source for time of flight experiments at IRMM, (unpublished).
13. G. Siebbens *et al.*, J. Radioanal. Nucl. Chem. **299**, 1093 (2014).
14. L. Csige *et al.*, Phys. Rev. C **87**, 044321 (2013).